16th World Conference on Earthquake Engineering, 16WCEE 2017
Santiago Chile, January 9th to 13th 2017
Paper N° 796
Registration Code: S- E1463038088

NONSMOOTH SEISMIC RESPONSE ANALYSIS OF A STRAIGHT BRIDGE WITH DECK ROTATION INDUCED BY ABUTMENT IMPACT

Z. Shi[(1)] and E.G. Dimitrakopoulos[(2)]

[(1)] Post-doctoral Fellow, The Hong Kong University of Science and Technology, zhongqishi@ust.hk / szqbell@gmail.com
[(2)] Assistant Professor, The Hong Kong University of Science and Technology, ilias@ust.hk

Abstract

The deck-abutment contact (e.g. pounding) during earthquake shaking often triggers the rotation of the deck. Contact at the deck level might alter dramatically the effective mechanical system activating unforeseen, in the design stage, behavior. This discrepancy between the assumed during design seismic behavior, and the actual seismic behavior governed by the nonsmooth planar deck dynamics, can be detrimental leading even to deck unseating/collapse. The impact-induced rotation mechanism is usually encountered in skew bridges, but it is observed also in straight bridges. As a reference, the 2013 experimental shake-table study of a four-span straight bridge by Saiidi et al. [1] showed unexpected large in-plane rotations. This resulted in significant residual displacement of the bents. The present paper simulates the response of that benchmark straight bridge in an attempt to capture the deck-abutment impact and the subsequent in-plane rotation. The study brings forward the (friction-based) physical mechanism behind the rotation of straight bridges which is usually ignored during design and analysis. In this context, it extends a previously established nonsmooth rigid body approach to account for the different excitations at the bottom of the bents and the abutments. The results shed light the role of friction on the impact-induced rotation mechanism, and underline the importance of devising practice-oriented procedures for considering during seismic design the potential in-plane deck rotation of even straight bridges. Finally, the study also investigates the sensitivity of the rotation with respect to the coefficient of friction value.

Keywords: nonsmooth dynamics, deck-abutment impact, deck rotation, concrete bridge, seismic response, pounding

1. Introduction

Contact (e.g. impact/pounding) either between adjacent deck segments or between deck and abutment occurs often during earthquakes [2, 3]. Contact has direct and indirect consequences on seismic response. A direct consequence is local damage: crushing of concrete around the contact area, shear-key damage, or even, abutment tilting. Often more important though, are the indirect consequences, since contact alters drastically the effective mechanical system, activating unforeseen, in the design stage, behavior. This discrepancy between the assumed seismic behavior during design, and the actual seismic behavior triggered by contact, can be detrimental for the bridge, leading even to deck unseating/collapse [4, 5, 6]. A characteristic example is the seismic response of skew bridges with joints, where due to the earthquake-induced pounding, skew deck segments tend to stick at the obtuse corner and rotate, as rigid bodies, in the direction of increasing the skew angle [4, 7]. Interestingly, this rotation-mechanism is not exclusive to skew bridges. Both straight, as well as, curved in-plan, segmental bridges, might suffer also from contact-induced rotations as certified by the Chi-Chi (1999) [8] and the Wenchuan (2008) [9] earthquake.

Motivated by the extensive damage after the 1971 San Fernando earthquake [4, 10], Maragakis et al. [11], examined analytically the deck-abutment interaction of short skew bridges. They [11] argued that the deck-abutment pounding could produce considerable in-plane deck rotations and subsequently transverse deck displacements. Following [11] many studies verified that a skew deck increases the possibility of coupling between the response displacements and the in-plane rotation (e.g. [12] among others). Further, [13] concluded that the deck-abutment contact reduced by two-thirds the ultimate load capacity of skew bridges and, in addition, it introduced failure mechanisms unseen to similar straight bridges. Kaviani et al. [14] noted the detrimental role of the skew angle on the deck rotations, on the column drift ratio and the collapse probability of the bridge.

Even though, the role of the in-plane dynamics of the deck, and the associated rotation mechanisms activated by the earthquake-induced pounding has been highlighted more than 20 years ago (e.g. [4]), it still has not received the attention it deserves in literature. A key study for the present research is the insightful 2013 experimental study [1] (large-scale shake-table tests) of a 4-span straight bridge. Saiidi et al. [1] reported significant in-plane rotation of the deck (maximum about 0.6°) triggered by deck-abutment contact, and leading to unexpected lateral displacements of the bents and severe damage to the columns. It is particularly interesting that the deck of the bridge was not skew. Among all potential influential factors, including the asymmetric stiffness and the slight spatial variation of the examined excitations, the frictional deck-abutment contact forces (and the produced torsional moment) were found to be the main reason of the (substantial) deck rotation about its vertical axis. In other words, [1] verified experimentally, for the first time, the potentially detrimental indirect consequences of (deck) contact in the seismic response of (straight) bridges.

Key of any numerical/analytical study of pounding bridge-segments is the simulation of the contact/ impact phenomenon at the deck level. Most studies model solely the behavior in the normal direction of contact, adopting a gap element ('compliance') approach; i.e. a stiff spring (sometimes combined with a dashpot) working only in compression and activated after the gap-closure. The deck-abutment interaction or in-deck contact is usually simulated either with a single gap element in each corner of the deck [15 ~ 18], or with multiple distributed gap elements aligned perpendicularly to the contact surface in [13, 14, 19, 20]. More sophisticated finite-element simulations have also been proposed for the pounding in segmental straight bridges [21, 22]. The recent study of [21] adopted a detailed three-dimensional finite-element model of the bridge and the contact between adjacent bridge girders.

Following a different approach, [23 ~ 25] deployed a nonsmooth dynamics framework to capture the pounding-induced in-plane rotation of skew bridges. The [23, 24] studies considered the unilateral contact/impact between a planar rigid body and a rigid half-space (the abutments), as the archetypal mechanical configuration of the deck-abutment impact. They revealed that the tendency of pounding deck segments to rotate depends on the total geometry of the deck in-plan, and not on the skew angle alone. Further, [23 ~ 25] showed that similar impact-rotation mechanisms characterize both frictionless impacts, as well as, the more complex case of frictional impacts.

The motivation for this study originates from the increased examples of (skew or straight) bridges suffering pounding-induced in-plane deck rotation and the associated need to comprehend the seismic deck-abutment contact interaction. In particular, the scope of the present paper is to advance our understanding of the contact-triggered rotation of the deck of straight bridges and the influence of friction. Such rotations are typically ignored in the design practice. In this context, the present study extends the nonsmooth dynamics framework of [23 ~ 25] in dealing with the multi-support excitation of the bents and the abutments of a bridge system.

2. Motivation and Background

Saiidi et al. [1] tested experimentally a conventional 4-span reinforced concrete (RC) bridge. The (1/4-scale) bridge model (Fig. 1) is a 32.2-m-long, 2.4-m-wide, RC bridge with a straight continuous post-tensioned superstructure supported on three 2-column bents. The different bent heights result in a slight eccentricity of the center with respect to the center of mass of the bridge. Independent shake tables control the acceleration (in both the longitudinal and the transverse directions) of each bridge bent at its base, while separate actuators control the displacement (solely in the longitudinal direction) of each abutment. The input excitation uses 7 sets of ground motion records, with the target peak ground acceleration (PGA) in the longitudinal direction varying from 0.09g to 1.20g. Note that the input excitations simulate historic ground motion records from the 1994 Northridge earthquake.

Of particular interest for the present study, is the substantial in-plane rotation reported in the experimental tests [1] despite the fact that the deck was not skew. During the first two excitations, no severe pounding occurs thus the recorded rotation is not large. These rotations are attributed to the stiffness asymmetry and the slightly different input ground motions among the three shake tables. However, during the later excitations the deck-abutment interaction becomes more severe. The peak response rotation reaches approximately values of 0.01 rad

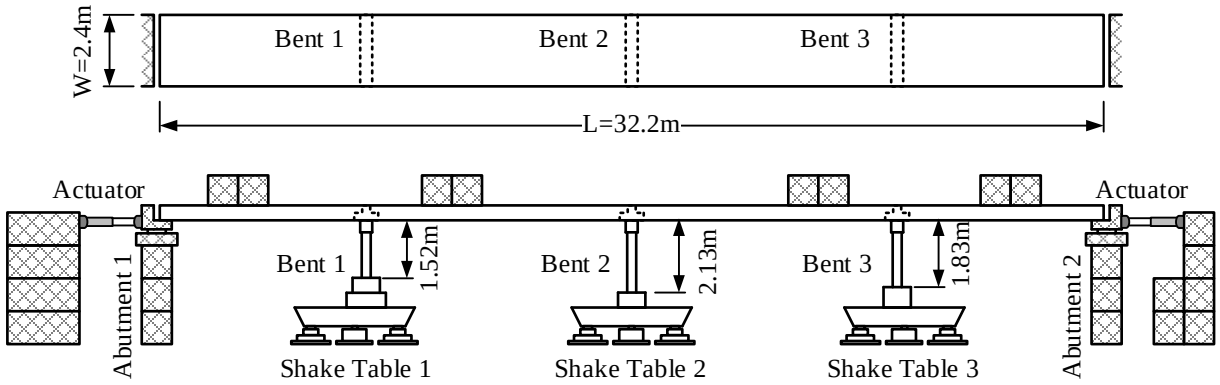

Fig. 1 – The 4-span straight bridge configuration tested experimentally in [1]

(0.63°) and the residual rotation values of about 0.005 rad (0.20°). Part of the motivation for the present study is to bring forward the physical mechanism behind these unexpectedly high rotations.

3. Proposed Approach

The two most commonly used methodologies for studying the impact phenomenon between adjacent structures (e.g. deck-abutment interaction) are: (a) the contact element (or compliance) approach, and (b) the nonsmooth approach. The former relies on the use of "contact/gap elements" comprised of a spring and a dashpot to simulate the impact force [26]. The present study adopts the latter methodology, which is a momentum-based method, and originates from multibody dynamics with unilateral contacts [27]. The proposed approach adopts the principles of nonsmooth dynamics and deploys an event-based analysis framework. An event-based methodology [28 ~ 30] decomposes the dynamic response into continuous motion (without impact) and discontinuous events such as impacts (i.e. instantaneous contact). Section 3.1 offers the equations of motion for the continuous smooth response, while Section 3.2 deals with the discontinuous nonsmooth events. Importantly, during impact, the proposed methodology focuses on the impulses transferred and bypasses the need to calculate the forces during impact which are unpredictable and frail in nature. On the contrary, during continuous contact, the impact forces enter the equation of motion in the form of Lagrange multipliers.

3.1 Smooth response

Consider the conceptual bridge model of Fig. 2, subjected to different ground motion excitations (multiple-support excitation u_{g1} ~ u_{g3}) at the three-bent supports and the two abutments. Let the motion of the system be described with respect to an absolute reference frame (denoted with superscript *a*). The (Newton-Euler) equation of motion for this multiple-support system with unilateral contacts can be expressed as:

$$\mathbf{M}\ddot{\mathbf{u}}^a - \mathbf{F}_D - \mathbf{F}_S - \begin{bmatrix}\mathbf{W}_N & \mathbf{W}_T\end{bmatrix}\begin{bmatrix}\boldsymbol{\lambda}_N \\ \boldsymbol{\lambda}_T\end{bmatrix} = 0 \tag{1}$$

where $\mathbf{M}$ is the mass matrix, $\mathbf{u}^a$ is the displacements vector with respect to the absolute system of reference, $\mathbf{F}_D$ and $\mathbf{F}_S$ are the vectors of the damping and the restoring force, $\mathbf{W}_N$ and $\mathbf{W}_T$ are the direction matrices of the contact (constraint) forces in the normal (subscript *N*) and the tangential (subscript *T*) direction, respectively. Subscripts "*N*" and "*T*" are used in the same way throughout the study. $\boldsymbol{\lambda}_N$ and $\boldsymbol{\lambda}_T$ are the contact force vectors along the two directions of contact and are treated as Lagrange multipliers. These contact forces enter the equation of motion only for active continuous contacts.

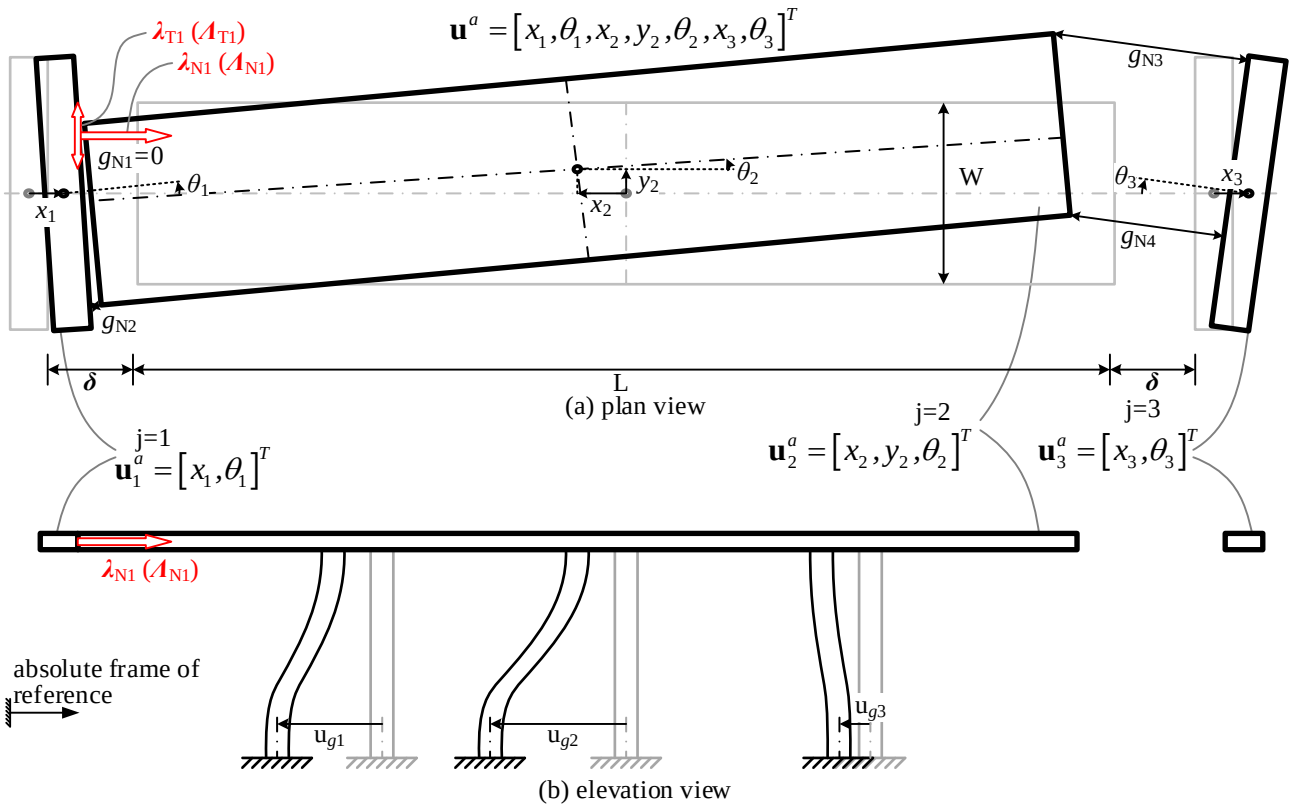

Fig. 2 – Deck-abutment rigid (unilateral) contact interaction

3.2 Nonsmooth contact events

Assume that during seismic excitation the deck and the abutments behave as rigid bodies with negligible structural deformation. This assumption is verified, at least for the deck, with the experimental results reported in [1]. In particular, the recorded response rotation (in [1]) of the left and the right halves of the deck is identical, indicating that indeed the structural deformation of the deck is negligible. Further, let the deck-abutment interaction follow the principles of unilateral contact [27], i.e. the contacting bodies cannot overlap; imposing a kinematic impenetrability constraint. Note that the local deformation the contacting bodies undergo at the impact points is assumed negligible in the body's scale [31].

Fig. 2 also shows the conceptual model of the examined bridge system (e.g. the left upper corner of the deck is in contact with the left abutment). The deck (rigid body $j = 2$) has three degrees of freedom ($\mathbf{u}_2 = [x_2, y_2, \theta_2]^T$): the two lateral translations along x and y axes, and one in-plane rotation. Recall that the abutments are excited individually by controlling their displacement along solely the longitudinal direction, but they rotate due to pounding during the experimental tests. Therefore, let x_1, x_3 and θ_1, θ_3 be the longitudinal displacement and the in-plane rotation of abutment "1" and "3" respectively. In summary, the generalized coordinates vector for the abutments and the deck with respect to an absolute reference frame (superscript a) has total 7 DOFs: $\mathbf{u}^a = [x_1, \theta_1, x_2, y_2, \theta_2, x_3, \theta_3]^T$. Subsequently, the relative distance vector ($\mathbf{g}_N$) can be expressed as:

$$\mathbf{g}_N = \mathbf{W}_N^T \mathbf{u}^a \tag{2}$$

The proposed approach departs from a conventional response history analysis once deck-abutment contact is detected. Contacts are distinguished into instantaneous (i.e. impacts) and of finite duration (i.e. continuous contacts) events. During impacts, all non-impulsive forces are considered negligible, wave effects within the body are ignored and the position of the contacting bodies is assumed fixed. Under these assumptions, impacts induce sudden, velocity changes ('jumps') making the response discontinuous (nonsmooth).

The proposed approach formulates both types of contacts (impacts and continuous contacts) as pertinent Linear Complementarity Problems (LCPs). A LCP consists of determining two unknown non-negative vectors $\mathbf{x} \geq \mathbf{0}$ and $\mathbf{y} \geq \mathbf{0}$ satisfying the complementarity condition: $\mathbf{y}^T\mathbf{x} = \mathbf{0}$, from a system of linear equations $\mathbf{y} = \mathbf{A}\mathbf{x} + \mathbf{b}$ with matrices $\mathbf{A}$ and $\mathbf{b}$ known [32] (see for example Eq. (6) and Eq. (9) in the following). The present study solves numerically the proposed LCPs with the aid of Lemke's pivotal algorithm [32]. As the study shows later on, the proposed LCPs encapsulate a great variety of post-impact states, such as impact, detachment, bouncing, full contact and transitions between different states (such as sliding and sticking contacts).

3.2.1 LCP for impact

Under the assumptions of this study, impacts result in instantaneous velocity changes ('jumps'). Thus, impact events are not described by the equation of motion (Eq. (1)). Instead, the integration of the equations of motion is interrupted, and the solution of the pertinent LCP returns the post-impact state, which becomes the new initial condition for the re-initiation of the time-integration.

The proposed approach adopts Newton's law in the normal direction of impact and Coulomb's friction law in the tangential direction. According to Newton's impact law the ratio of the relative normal contact velocity vector before ($\dot{\mathbf{g}}_N^-$) and after impact ($\dot{\mathbf{g}}_N^+$), is equal with the coefficient of restitution $\boldsymbol{\varepsilon}_N$:

$$\dot{\mathbf{g}}_N^+ = -\boldsymbol{\varepsilon}_N \dot{\mathbf{g}}_N^- \tag{3}$$

Let $\mathbf{v}_N$ denote velocity jumps along the normal direction of contact:

$$\mathbf{v}_N = \dot{\mathbf{g}}_N^+ + \boldsymbol{\varepsilon}_N \dot{\mathbf{g}}_N^- \tag{4}$$

The LCP which captures the impact-induced velocity jumps, treats frictional impacts on a velocity level (see also [23 ~ 25]) and encompasses different impact states such as slip, stick and reversal of sign, both for single and double impacts:

$$\begin{pmatrix} \mathbf{v}_N \\ \dot{\mathbf{g}}_{TR}^+ \\ \boldsymbol{\Lambda}_{TL} \end{pmatrix} = \begin{pmatrix} \mathbf{G}_{NN} - \mathbf{G}_{NT}\bar{\bar{\boldsymbol{\mu}}} & \mathbf{G}_{NT} & \mathbf{0} \\ \mathbf{G}_{TN} - \mathbf{G}_{TT}\bar{\bar{\boldsymbol{\mu}}} & \mathbf{G}_{TT} & \mathbf{E} \\ 2\bar{\bar{\boldsymbol{\mu}}} & -\mathbf{E} & \mathbf{0} \end{pmatrix} \times \begin{pmatrix} \boldsymbol{\Lambda}_N \\ \boldsymbol{\Lambda}_{TR} \\ \dot{\mathbf{g}}_{TL}^+ \end{pmatrix} + \begin{pmatrix} \left(\bar{\bar{\boldsymbol{\varepsilon}}}_N + \mathbf{E}\right)\dot{\mathbf{g}}_N^- \\ \mathbf{E}\dot{\mathbf{g}}_T^- \\ \mathbf{0} \end{pmatrix} \tag{5}$$

$$\begin{pmatrix} \mathbf{v}_N \\ \dot{\mathbf{g}}_{TR}^+ \\ \boldsymbol{\Lambda}_{TL} \end{pmatrix} \geq \mathbf{0}, \begin{pmatrix} \boldsymbol{\Lambda}_N \\ \boldsymbol{\Lambda}_{TR} \\ \dot{\mathbf{g}}_{TL}^+ \end{pmatrix} \geq \mathbf{0}, \text{ and } \begin{pmatrix} \mathbf{v}_N \\ \dot{\mathbf{g}}_{TR}^+ \\ \boldsymbol{\Lambda}_{TL} \end{pmatrix}^T \begin{pmatrix} \boldsymbol{\Lambda}_N \\ \boldsymbol{\Lambda}_{TR} \\ \dot{\mathbf{g}}_{TL}^+ \end{pmatrix} = \mathbf{0} \tag{6}$$

where $\bar{\bar{\boldsymbol{\mu}}} = \text{diag}\{\mu_i\}$ is Coulomb's coefficient of friction and $\bar{\bar{\boldsymbol{\varepsilon}}} = \text{diag}\{\varepsilon_{Ni}\}$ with i being the index of the impact points, $\boldsymbol{\Lambda}_N$ and $\boldsymbol{\Lambda}_T$ stand for the normal and the tangential impulse, $\dot{\mathbf{g}}_{TR}^+$ and $\dot{\mathbf{g}}_{TL}^+$ are the positive and the negative parts of the tangential post-impact velocity (see also [23 ~ 25]), $\dot{\mathbf{g}}_T^-$ is the tangential pre-impact velocity; $\mathbf{E}$ is the identity matrix, and the $\mathbf{G}$ matrices are:

$$\begin{aligned} \mathbf{G}_{NN} &= \mathbf{W}_N^T\mathbf{M}^{-1}\mathbf{W}_N, \ \mathbf{G}_{NT} = \mathbf{W}_N^T\mathbf{M}^{-1}\mathbf{W}_T \\ \mathbf{G}_{TN} &= \mathbf{W}_T^T\mathbf{M}^{-1}\mathbf{W}_N, \ \mathbf{G}_{TT} = \mathbf{W}_T^T\mathbf{M}^{-1}\mathbf{W}_T \end{aligned} \tag{7}$$

3.2.2 LCP for continuous contact and detachment

On the contrary, continuous contacts produce contact forces of finite magnitude and duration which enter the equations of motion (Eq. (1) through the $\boldsymbol{\lambda}$ vector) as Lagrange multipliers. When the state of contact changes, e.g. a transition occurs between sticking/sliding contact, or from closed to open contact (named detachment), the

value of the contact forces and the corresponding new initial conditions are determined with the aid of the pertinent LCP, established on the acceleration level. Specifically, let $\boldsymbol{\lambda}_N$ denote the contact force vector along the normal direction of contact and $\boldsymbol{\lambda}_H$ the frictional force vector of sticking contacts along the tangential direction. Then the LCP that treats continuous contact and detachment is:

$$\begin{pmatrix} \ddot{\mathbf{g}}_N \\ \ddot{\mathbf{g}}_{HL} \\ \bar{\bar{\boldsymbol{\mu}}}_H \boldsymbol{\lambda}_N + \boldsymbol{\lambda}_H \end{pmatrix} = \begin{pmatrix} \mathbf{W}_N^T \mathbf{M}^{-1} \mathbf{W}_Q & -\mathbf{W}_N^T \mathbf{M}^{-1} \mathbf{W}_H & \mathbf{0} \\ -\mathbf{W}_H^T \mathbf{M}^{-1} \mathbf{W}_Q & \mathbf{W}_H^T \mathbf{M}^{-1} \mathbf{W}_H & \mathbf{E} \\ 2\bar{\bar{\boldsymbol{\mu}}}_H & -\mathbf{E} & \mathbf{0} \end{pmatrix} \times \begin{pmatrix} \boldsymbol{\lambda}_N \\ \bar{\bar{\boldsymbol{\mu}}}_H \boldsymbol{\lambda}_N - \boldsymbol{\lambda}_H \\ \ddot{\mathbf{g}}_{HR} \end{pmatrix} + \begin{pmatrix} \mathbf{W}_N^T \mathbf{M}^{-1} \mathbf{h} \\ -\mathbf{W}_N^T \mathbf{M}^{-1} \mathbf{h} \\ \mathbf{0} \end{pmatrix} \tag{8}$$

$$\begin{pmatrix} \ddot{\mathbf{g}}_N \\ \ddot{\mathbf{g}}_{HL} \\ \bar{\bar{\boldsymbol{\mu}}}_H \boldsymbol{\lambda}_N + \boldsymbol{\lambda}_H \end{pmatrix} \geq \mathbf{0}, \begin{pmatrix} \boldsymbol{\lambda}_N \\ \bar{\bar{\boldsymbol{\mu}}}_H \boldsymbol{\lambda}_N - \boldsymbol{\lambda}_H \\ \ddot{\mathbf{g}}_{HR} \end{pmatrix} \geq \mathbf{0}, \text{ and } \begin{pmatrix} \ddot{\mathbf{g}}_N \\ \ddot{\mathbf{g}}_{HL} \\ \bar{\bar{\boldsymbol{\mu}}}_H \boldsymbol{\lambda}_N + \boldsymbol{\lambda}_H \end{pmatrix}^T \begin{pmatrix} \boldsymbol{\lambda}_N \\ \bar{\bar{\boldsymbol{\mu}}}_H \boldsymbol{\lambda}_N - \boldsymbol{\lambda}_H \\ \ddot{\mathbf{g}}_{HR} \end{pmatrix} = \mathbf{0} \tag{9}$$

with,

$$\mathbf{W}_Q = \mathbf{W}_N + \mathbf{W}_G \bar{\bar{\boldsymbol{\mu}}}_G + \mathbf{W}_H \bar{\bar{\boldsymbol{\mu}}}_H \tag{10}$$

where $\ddot{\mathbf{g}}_N$ is the relative (contact) acceleration vector in the normal direction $\ddot{\mathbf{g}}_{HR}$ and $\ddot{\mathbf{g}}_{HL}$ the positive and the negative parts of the tangential (contact) acceleration vectors respectively. $\mathbf{W}_H$ and $\mathbf{W}_G$ are the direction matrices, and $\bar{\bar{\boldsymbol{\mu}}}_H$ and $\bar{\bar{\boldsymbol{\mu}}}_G$ are the diagonal matrices with the coefficients of friction for the potential sticking contacts (subscript *H*) and sliding contacts (subscript *G*).

4. Numerical Simulation of Pounding-Induced Rotation

4.1 Analytical modelling

The proposed methodology (Chapter 3) is implemented on the 4-span straight bridge [1, 33] (of Chapter 2). Fig. 3 presents the global model, including the deck, the two abutments and their actuators, and the six columns. There are 4 potential contacts (g_{N1} to g_{N4}). The motion of the left abutment, the deck and the right abutment are expressed by $\mathbf{u}_1 = [x_1, \theta_1]^T$, $\mathbf{u}_2 = [x_2, y_2, \theta_2]^T$ and $\mathbf{u}_3 = [x_3, \theta_3]^T$, respectively, based on the rigid-body assumption (Section 3.2). The mechanical configuration of Fig. 3 is subjected successively to seven excitations, reproducing the testing procedure followed in the experiments of [1].

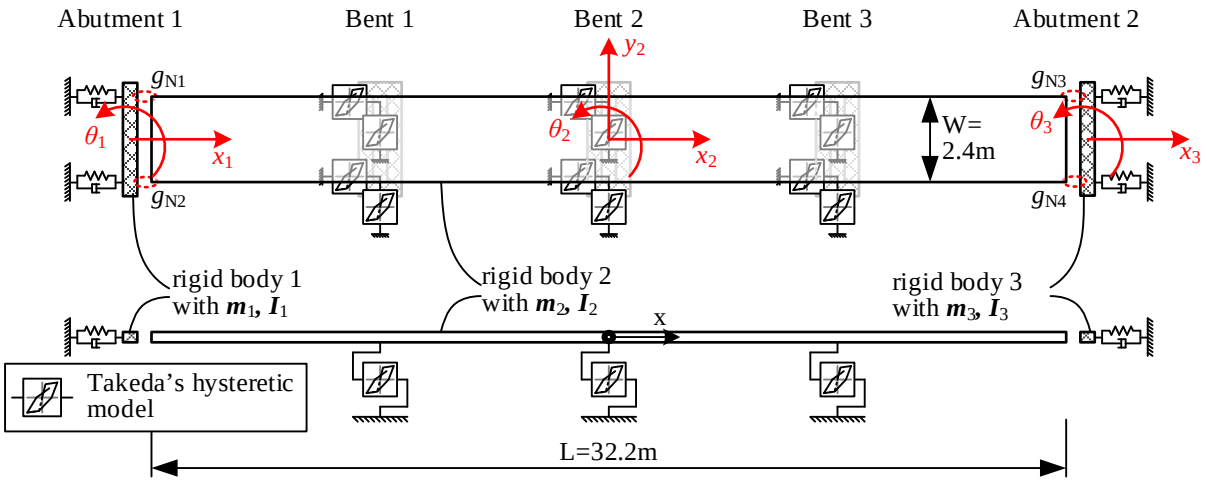

Fig. 3 – Analytical model of the 4-span straight bridge with 4 contact points

The concentrated mass at the center of the deck, including the additional mass blocks upon the deck, is $\boldsymbol{m}_2$ = 140.5 t for the translational directions while the mass moment of inertia about the vertical axis is $\boldsymbol{I}_2$ = 13090 t·m^2 (see [1, 33]). For all 6 columns, Takeda hysteretic models [34] with initial stiffness equal with the post-crack stiffness are assigned along both the longitudinal and the transverse directions, and an elastic torsional stiffness behavior is assumed.

The abutments are modelled as planar rigid blocks ($\boldsymbol{m}_1 = \boldsymbol{m}_3$ = 0.65 t and $\boldsymbol{I}_1 = \boldsymbol{I}_3$ = 0.31 t·m^2) connected to two sets of translational spring-damper systems, simulating the longitudinal and rotational stiffness and damping properties of the actuator behind each abutment. The deck-abutment interaction is treated as unilateral contact according to the proposed nonsmooth approach (refer to Section 3.2). The initial gap between deck and abutment is designed as 0.0127 m in the experimental test [1]. However, during the successive experimental tests the gap sizes varies. Thus, the initial gap values during the analysis are updated to match the measured gap sizes at the 4 corners at the beginning of each excitation. Rayleigh damping is applied as in [33], calculating the mass and the stiffness proportional coefficients for 2% damping at the first and the third mode. The assumed base excitation of each bent is the measured displacement of the shake tables during the tests. The input in the longitudinal and the rotational directions of the two abutments is back-calculated from the experimental measurements of the gap [1].

4.2 Preliminary analysis ignoring deck-abutment interaction

Before simulating the actual response recorded during the shake table tests, which includes the nonsmooth deck-abutment interaction, the simulation of the smooth response is first examined. Specifically, the proposed

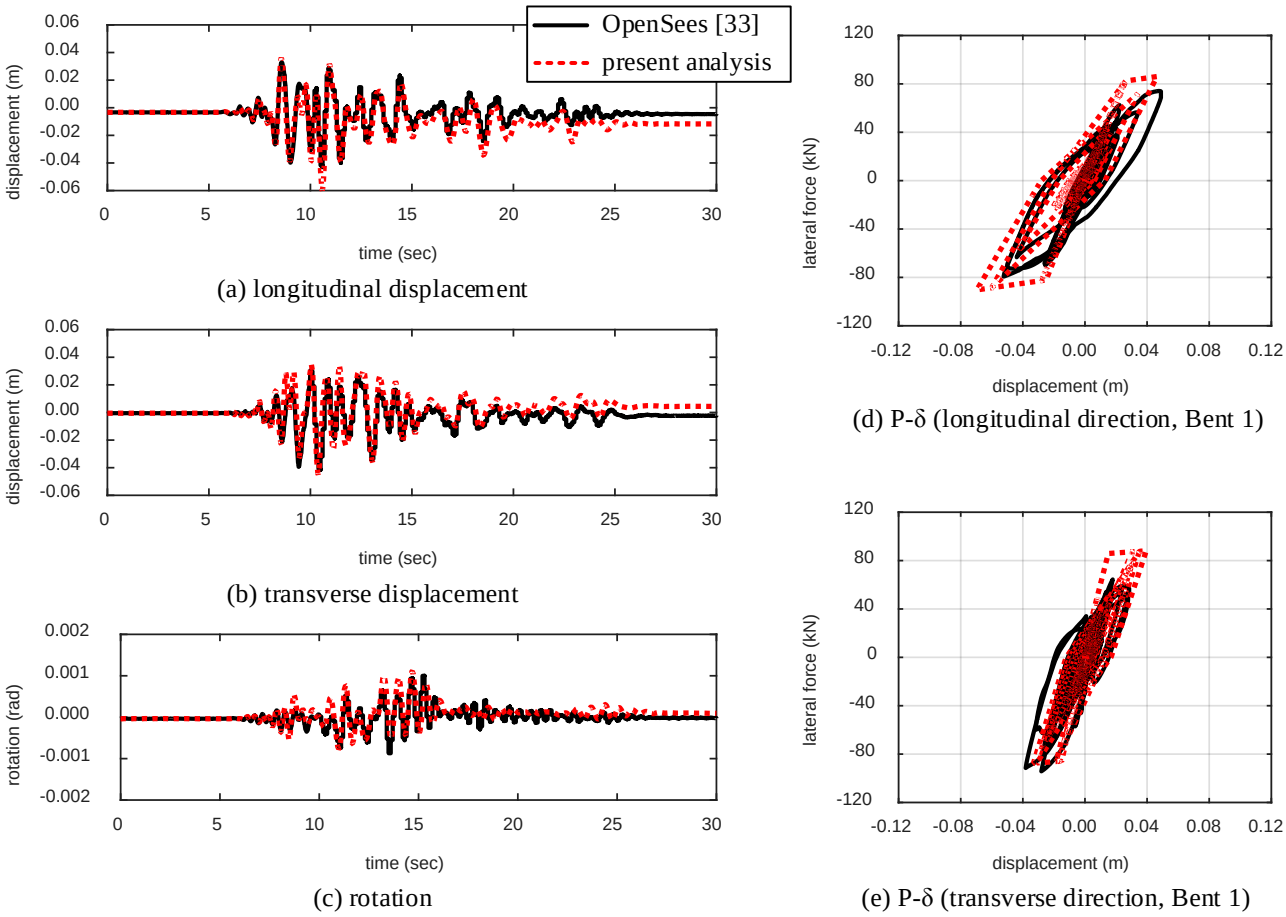

(a) longitudinal displacement

(b) transverse displacement

(c) rotation

(d) P-δ (longitudinal direction, Bent 1)

(e) P-δ (transverse direction, Bent 1)

Fig. 4 – Comparison of calculated response ignoring the deck-abutment interaction during Excitation No. 4: OpenSees [33] vs. proposed analysis

analytical model (of 7 DOFs) is compared with a pertinent OpenSees model of the same bridge system from [33] both ignoring the deck-abutment interaction. Fig. 4 shows the response history of the translational displacement (Fig. 4 (a) ~ (b)) and the rotation of the deck (Fig. 4 (c)). In addition, Fig. 4 (d) ~ (e) plots the force-displacement loops of one column of Bent 1 (as an example), as calculated with the present model and with the fiber modelling of [33]. All results of Fig. 4 concern the response during Excitation No. 4, which is characterized by moderate PGAs in the longitudinal and the transverse directions (respectively 0.60g and 0.50g) compared with the other six excitations considered in this study.

Fig. 4 (a) ~ (c) illustrates that the longitudinal displacement, the transverse displacement and the rotation in the proposed analysis generally match the OpenSees results. However, note that differences between the residual values among the two simulations exist and they are more important in the presence of the deck-abutment interaction later on. Also, Fig. 4 (d) ~ (e) shows that in general the proposed analysis leads to somewhat higher restoring force. This is attributed to the fact that the adopted column modelling considers the post-crack stiffness of the column as the initial stiffness and ignores the biaxial interaction. However, the vibration characteristics of the deck, as well as, the peak response are well captured by the proposed analysis. The results for the other six excitations are similar, but omitted for brevity.

4.3 Proposed seismic response analysis including the deck-abutment interaction

This section presents the response as calculated with the proposed approach (Section 3.2), taking into account the deck-abutment interaction. As a first approach the coefficient of friction is taken as $\mu = 0.5$ (later a

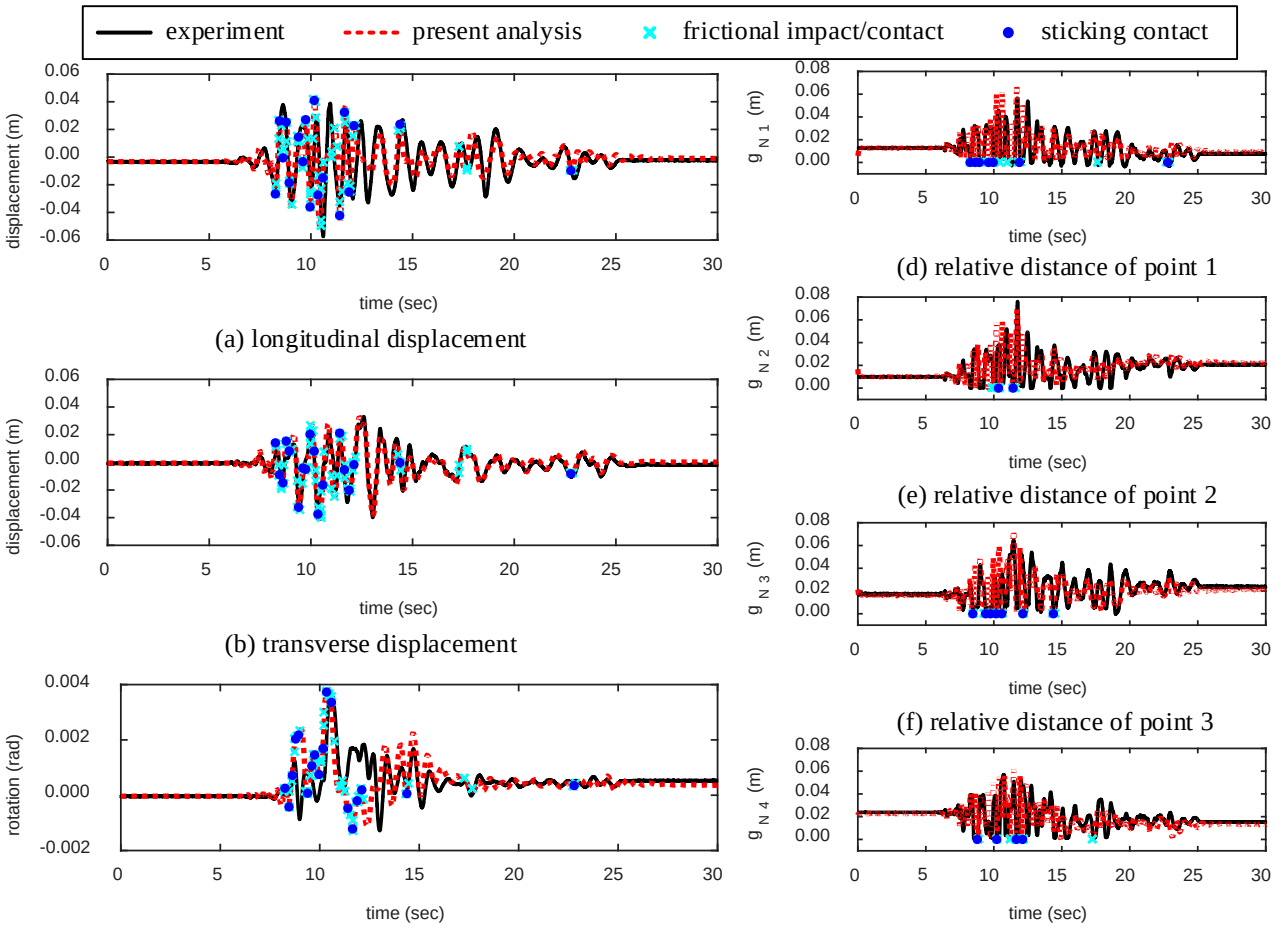

Fig. 5 – Comparison of response-history with deck-abutment interaction during Excitation No. 4: experiment [1] vs. proposed analysis

parametric study about μ is performed). Noticing that during the experimental test contacts were continuous (meaning of finite duration), the coefficient of restitution (ε) is estimated as zero.

The experimental and the (proposed) analytical results of Fig. 5 are based on the following calculation assumptions: The longitudinal response displacement of the deck is taken as the average of the two displacements measured at the two ends of the deck. The transverse displacement is equal with the one measured at the middle of the deck, and the in-plane rotation is calculated from two transverse displacements measured at two ends of the deck. The input motion of the abutments is back-calculated from the measured relative distance between the abutment and the deck. The spring-damper properties of each abutment represent the behavior of the actuator which is solely active in the longitudinal direction. The stiffness of the springs are calculated from the measured force (via load cell) and displacement during the experiments [1]. The rotation of the abutment is the result of deck-abutment contact.

Fig. 5 compares the analytical with the experimental results for Excitation No. 4. All contact events (i.e. frictional impacts/contacts) are indicated with crosses. Sticking contacts in particular (including both the immediate sticking contact after an impact, and the transition from a sliding contact into a sticking contact), are shown with filled blue circles. The events at all 4 points are plotted simultaneously for the response of the deck in Fig. 5 (a) ~ (c), while the events at solely each contact point are plotted for the pertinent relative distance in Fig. 5 (d) ~ (g). Fig. 5 (a) and (b) show that the current simulation reproduces well the response of deck in both the longitudinal and the transverse directions. The calculated rotation of the deck (Fig. 5 (c)) is in close agreement with the experimental results until about 11.0 sec, when the peak deck rotation occurs. Hence, the proposed analysis provides a good estimation of the peak deck rotation, despite the multiple (discontinuous) contact events preceding the appearance of the peak. From about 11.0 to 13.0 sec the analytical cannot match the experimental results. Fig. 5 (d) ~ (k) plots the relative gap distances and again, the proposed simulation is, in general, in good agreement with the experimental results. The conclusions from the comparison of the remaining six excitations are similar, but are omitted for brevity.

Further, Fig. 6 compares the deck response at 10.02 sec during Excitation No. 4 when the in-plane deck rotation starts increasing rapidly, to elucidate the contact-induced rotation mechanism. At this particular time instant, the deck is (according to the proposed analysis) moving toward left (v_{x2} = -0.0099 m/s) and upward (v_{y2} = +0.0038 m/s), with an anti-clockwise angular velocity of $v_{\theta 2}$ = 0.0076 rad/s. The deck (at Point 1) is sticking with the left abutment. The frictional force (λ_{T1} = 530 kN) prevents the left end of the deck from moving upward, resulting in further anti-clockwise in-plane rotation of the deck.

Fig. 7 summarizes the peak deck rotation (for all 7 excitations) versus the PGA of the input motion in the transverse direction. For reasons of comparison with [1], the abscissa of Fig. 7 reads in terms of the target PGA and not the feedback PGA (i.e. the one actually recorded during the tests). According to the experimental tests [1] the peak rotation increases exponentially with PGA. The calculated peak in-plane rotation ignoring the deck-abutment interaction (see Section 4.2), also superimposed in Fig. 7, exhibits a different trend. When the deck-abutment interaction is ignored the peak deck rotation is approximately proportional to the PGA, and noticeably smaller than that when the deck-abutment interaction is considered. This observation, together with Fig. 6, indicates the contact-induced frictional forces increase notably the tendency of the deck to rotate in-plane. The

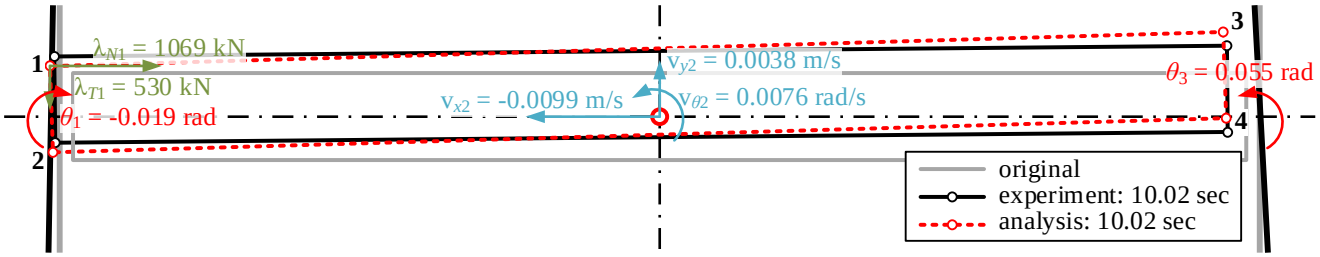

Fig. 6 – Comparison of deck response during Excitation No. 4: proposed analysis (deformation, response velocities, contact forces) vs. experimental result [1] (deformation only)

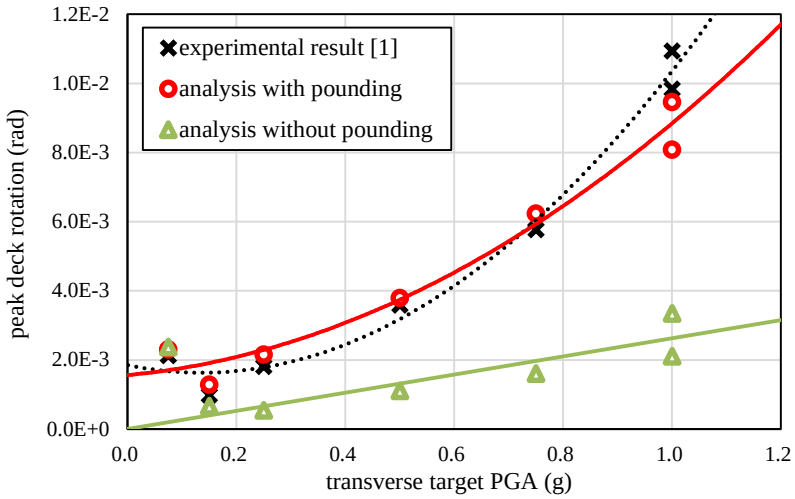

Fig. 7 – Peak deck rotation vs. target PGA

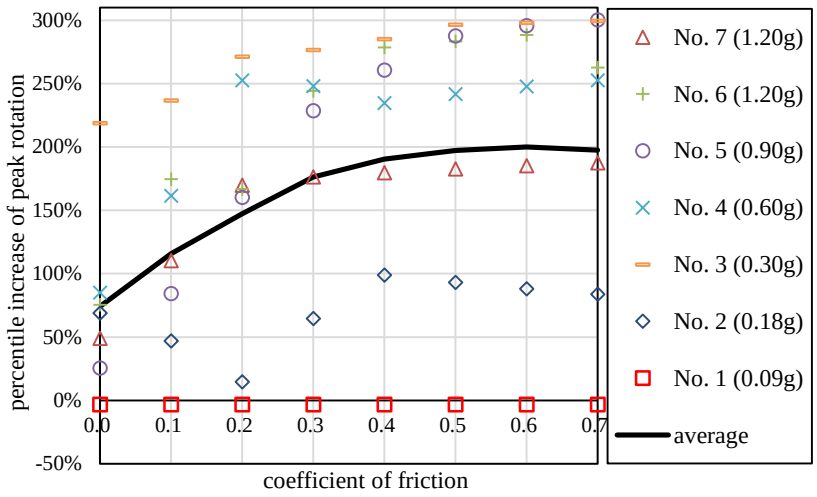

Fig. 8 – Percentile increase of peak rotation vs. coefficient of friction

proposed approach reproduces closely the same pattern with the experimental results, within some reasonable accuracy, in spite of the particular discrepancies in the response-history of some excitation cases (e.g. in Fig. 5).

Overall, the qualitative but also quantitative comparison between the analytical and the experimental results verifies the ability of the proposed approach to capture the deck-abutment interaction. Note the multiple sources of uncertainty between the proposed herein analytical approach and the independent experimental study which might directly and/or indirectly affect the comparison. For instance, several parameters, such as the coefficient of friction which is assumed as constant in the proposed analysis, may vary significantly even during the same excitation as the deck rotation changes and the contact area is damaged locally. The observed discrepancies pinpoint directions of further research but also might indicate the sensitivity of the contact-induced in-plane rotation.

4.4 Parametric study on coefficient of friction

This section investigates the sensitivity of the in-plane rotation of the deck to the coefficient of friction value. Specifically, Fig. 8 plots the percentile increase of the peak rotations (for all 7 excitations) compared to the peak

rotation without deck-abutment interaction (Section 4.2), versus the coefficient of friction (μ). The examined values of the coefficient of friction range from 0.0 to 0.7 with a 0.1 interval. The PGA in the longitudinal direction is shown in the parenthesis. The thick continuous line represents the average increase. Excitation No. 1 (PGA = 0.09g) does not result in increased in-plane rotation, since the contacts between the deck and the abutment are not severe. On the other hand, the increase of the peak rotation for the remaining six excitations is significant. Excitations No. 3 and No. 4 yield the highest increase even though they are of moderate PGAs; the peak rotation increases by approximately 3 times when $\mu = 0.5$, 0.6 or 0.7. In general, the peak rotation rises rapidly with the coefficient of friction until $\mu = 0.4$. For higher values of the coefficient of friction, the peak rotation saturates at around 200%.

5. Conclusions

The present paper deploys a nonsmooth rigid body approach, for the response-history analysis of a bridge system with multi-support excitation at the bottom of the bents and the abutments. The proposed analysis simulates the response of a benchmark straight bridge, tested experimentally by other researchers. The study brings forward the physical mechanism behind the rotation of straight bridges taking into account the frictional deck-abutment contact and the consequential in-plane rotation of the deck.

Overall, the proposed analysis captures qualitatively the contact-induced rotational behavior of the deck, and quantitatively reproduces, with reasonable accuracy, the peak rotations recorded during the benchmark experimental test. Discrepancies in the rotation response-history between the analytical and the experimental results are also noted. The results underline the importance of devising practice-oriented procedures for considering during seismic design the potential in-plane deck rotation of even straight bridges, even for straight bridges and shed light on the role of friction on the contact-induced rotation mechanism. The study also investigates the sensitivity of the contact-induced rotations to the values of the coefficient of friction. The results suggest that the peak rotation increases rapidly with the coefficient of friction μ when μ is smaller than 0.4, but saturates for higher values.

6. References

[1] Saiidi MS, Vosooghi A, Nelson R (2013): Shake-table studies of a four-span reinforced concrete bridge. *Journal of Structural Engineering, ASCE*, **139**, 1352–1361.

[2] Kosa K, Sazaki K, Yamaguchi E (2002): Mechanism of damage to Shiwei Bridge caused by 1999 Chi-Chi earthquake. *Structural Engineering/Earthquake Engineering, JSCE*, **19** (2), 221s-226s.

[3] Buckle I, Hube M, Chen G, Yen W, Arias J (2012): Structural performance of bridges in the Offshore Maule earthquake of 27 February 2010. *Earthquake Spectra*, **28** (S1), S533-S552.

[4] Priestley MN, Seible F, Calvi GM (1996): *Seismic design and retrofit of bridges*. John Wiley & Sons.

[5] Kawashima K, Takahashi Y, Ge H, Wu Z, Zhang J (2009): Reconnaissance report on damage of bridges in 2008 Wenchuan, China, earthquake. *Journal of Earthquake Engineering*, **13**, 965-996.

[6] Yashinsky M, Karshenas MJ (2003): *Fundamental of seismic protection for bridge*. Earthquake Engineering Research Institute.

[7] Kawashima K, Unjoh S, Hoshikuma J, Kosa K (2011): Damage of bridges due to the 2010 Maule, Chile, earthquake. *Journal of Earthquake Engineering*, **15** (7), 1036-1068.

[8] Chang KC, Chang DW, Tsai MH, Sung YC (2000): Seismic performance of highway bridges. *Earthquake engineering and engineering seismology*, **2**, 55-77.

[9] Zhang H, Li J, Saiidi MS (2011): Evaluation of performance of a skew bridge in Wenchuan 2008 earthquake. *the International Symposium on Engineering Lessons Learned from the 2011 Great East Japan Earthquake*. Tokyo, Japan.

[10] Wood J, Jennings P (1971): Damage to freeway structures in the San Fernando earthquake. *Bulletin of the New Zealand Society for Earthquake Engineering*, **4**, 347-376.

[11] Maragakis EA, Jennings PC (1987): Analytical models for the rigid body motions of skew bridges. *Earthquake engineering & structural dynamics*, **15**, 923-944.

[12] Kwon O, Jeong S (2013): Seismic displacement demands on skewed bridge decks supported on elastomeric bearings. *Journal of Earthquake Engineering*, **17**, 998-1022.

[13] Bignell JL, LaFave JM, Hawkins NM (2005): Seismic vulnerability assessment of wall pier supported highway bridges using nonlinear pushover analyses. *Engineering structures*, **27**, 2044-2063.

[14] Kaviani P, Zareian F, Taciroglu E (2012): Seismic behavior of reinforced concrete bridges with skew-angled seat-type abutments. *Engineering Structures*, **45**, 137-150.

[15] Maragakis EA, Thornton G, Saiidi M, Siddharthan RA (1989): Simple non-linear model for the investigation of the effects of the gap closure at the abutment joints of short bridges. *Earthquake Engineering & Structural Dynamics*, **18**, 1163-1178.

[16] Kawashima K, Tirasit P (2008): Effect of nonlinear seismic torsion on the performance of skewed bridge piers. *Journal of Earthquake Engineering*, **12**, 980-998.

[17] Maleki S (2005): Seismic modeling of skewed bridges with elastomeric bearings and side retainers. *Journal of bridge Engineering*, **10**, 442-449.

[18] Watanabe G, Kawashima K (2004): Effectiveness of cable-restrainer for mitigating rotation of a skewed bridge subjected to strong ground shaking, *13th World Conference on Earthquake Engineering*, Vancouver, Canada.

[19] Huo Y, Zhang J (2013): Effects of pounding and skewness on seismic responses of typical multispan highway bridges using the fragility function method. *Journal of Bridge Engineering, ASCE*. **18** (6), 499-515.

[20] Abdel-Mohti A, Pekcan G (2008): Seismic response of skewed RC box-girder bridges. *Earthquake Engineering and Engineering Vibration*, **7**, 415-426.

[21] Bi K, Hao H (2013): Numerical simulation of pounding damage to bridge structures under spatially varying ground motions. *Engineering Structures*, **46**, 62-76.

[22] Zhu P, Abe M, Fujino Y (2002): Modelling three-dimensional non-linear seismic performance of elevated bridges with emphasis on pounding of girders. *Earthquake engineering & structural dynamics*, **31**, 1891-1913.

[23] Dimitrakopoulos EG (2010): Analysis of a frictional oblique impact observed in skew bridges. *Nonlinear Dynamics*, **60**, 575-595.

[24] Dimitrakopoulos EG (2011): Seismic response analysis of skew bridges with pounding deck-abutment joints. *Engineering Structures*, **33**, 813–826.

[25] Dimitrakopoulos E (2013): Nonsmooth analysis of the impact between successive skew bridge-segments. *Nonlinear Dynamics*, **74**, 911-928.

[26] Guo A, Cui L, Li S, Li H (2015): A phenomenological contact-element model considering slight non-uniform contact for pounding analysis of highway bridges under seismic excitations. *Earthquake Engineering & Structural Dynamics*, **44**, 1677-1695.

[27] Pfeiffer F, Glocker C (2004): *Multibody dynamics with unilateral contacts*. Weinheim: Wiley-VCH.

[28] Leine RI, Van Campen DH, Glocker CH (2003): Nonlinear dynamics and modeling of various wooden toys with impact and friction. *Journal of Vibration Control*, **9** (1–2), 25–78.

[29] Glocker C (2001): *Set-Valued Force Laws*. Springer.

[30] Brogliato B (1999): *Nonsmooth mechanics: models, dynamics and control*. Springer.

[31] Andreaus U, Casini P (1999): On the rocking-uplifting motion of a rigid block in free and forced motion: influence of sliding and bouncing. *Acta Mechanica*, **138**, 219-241.

[32] Cottle R, Pang J, Stone RE (1992): *The linear complementarity problem*. Boston: Academic Press.

[33] Zadeh M, Saiidi M (2007): Pre-test analytical studies of NEESR-SG 4-span bridge model using OpenSees, *Report No. CCEER-07-3*, Center for Civil Engineering Earthquake Research, Department of Civil Engineering, University of Nevada, Reno.

[34] Takeda T, Sozen MA, Nielsen NN (1970): Reinforced concrete response to simulated earthquakes. *Journal of Structural Division, ASCE*, **96** (12), 2557-2573.